Chemical Engineering Journal 323 (2017) 252–259

Contents lists available at ScienceDirect

Chemical Engineering Journal

journal homepage: www.elsevier.com/locate/cej

Tunable construction of multi-shell hollow SiO_2 microspheres with hierarchically porous structure as high-performance anodes for lithium-ion batteries

Xiaoming Ma *, Zipeng Wei, Huijuan Han, Xiaobing Wang, Kaiqing Cui, Lin Yang

Collaborative Innovation Center of Henan Province for Green Manufacturing of Fine Chemicals, Ministry of Education, School of Chemistry and Chemical Engineering, Henan Normal University, Xinxiang, Henan 453007, PR China

HIGHLIGHTS

- Multi-shell hollow SiO_2 microspheres with hierarchical porous are tunably obtained.
- The materials have the unique hollow multi-shell and hierarchical porous structure.
- The preparation method is simple and repeatable.
- The silica materials exhibit excellent rate capacity and cycling performance.

ARTICLE INFO

Article history:
Received 13 February 2017
Received in revised form 14 April 2017
Accepted 24 April 2017
Available online 25 April 2017

Keywords:
Multi-shell hollow materials
Hierarchically porous structure
Silica
Lithium ion battery

ABSTRACT

Silica is one of the most abundant materials on the earth, and promises a high potential application in lithium ion battery (LIB). The crucial challenge for SiO_2 materials is the huge volume change and poor electrical conductivity during the lithiation and delithiation process which result into the rapid capacity fading and bad cyclability. Herein, we successfully synthesized the multi-shell hollow silica microspheres (MHSM) with hierarchically porous structure via a simple sacrificial template method. The numbers of shell could be simply controlled by the precursor (Na_2SiO_3) loading. The multi-shell and hierarchically porous structure could endow SiO_2 with large volume, good porosity and permeability. These advantages could offer not only the plentiful electrode-electrolyte reaction sites but also a "buffer" to hinder the volume expansion of silica in the Li^+ charge-discharge process. The research results showed that LIB assembled with the MHSM exhibited high capacity and long cycle life. The multi-shell and hierarchically porous structures provide a novel morphology of anode materials to enhance rate capability and structural stability of high-capacity electrode materials.

1. Introduction

Lithium ion batteries (LIB), with the rapid development of portable electronic devices and electrical vehicles, have become one of the dominant power sources due to their high energy density, light weight and environment friendly devices [1–4]. In the numerous LIB anodes, the silicon-based materials have drawn a great attention of the researchers due to their high theoretical specific capacity and low operating voltage [5–8]. Especially SiO_2, it has become the focus of attention due to high theoretical special capacity and low discharge potential in the lithium ion storage comparing with the traditional graphite materials and other commercial electrode materials. Meanwhile, because of the complexity, difficulty and instability of the synthesis of Si, SiO_2 materials as LIB anodes had been considered to be an alternative material of Si, and it had also similar advantages with Si such as: ① high Li-storage capacity; ② low discharge potential. In addition, the cost for the silica as the LIB anodes is cheaper than other materials, because SiO_2 is one of the most abundant materials on Earth [9,10]. Up to now, some SiO_2 materials with different morphologies, such as nanoparticle [11], thin film [12] and nanocube [13], were used for the field of lithium ion battery and possessed good property. However, the tremendous volume expansion and poor electrical conductivity of SiO_2 materials could result into unstable long-time cycle performance during the lithiation and delithiation process and it is urgently need to construct the SiO_2 materials with special structure to improve the electrochemical performance [14–16].

* Corresponding author.
E-mail address: sunshinyma@hotmail.com (X. Ma).

http://dx.doi.org/10.1016/j.cej.2017.04.108
1385-8947/

Due to the high surface area, large pore volume and low density, multi-shell hollow materials with hierarchical pores may have potential applications in photocatalysis [17] and drug delivery [18]. Especially, comparing with the single-size porous structure, the hierarchical pores structure, formed by the hierarchical and orderly assembly of different sizes pores, make the materials possess better porosity and permeability [19]. The multi-shell and hierarchically porous structure could hinder the volume expansion and improve the electrical conductivity of silica via the buffer function of pore-by-pore and shell-by-shell [20,21]. For example, Co_3O_4 with multishelled hollow structure exhibited good rate capacity, cycling performance, and an ultrahigh specific capacity through a template method [22,23]. The superior cyclic stability and capacity resulted from the synergetic effect of small diffusion lengths in the building blocks and sufficient void space to buffer the volume expansion. The advantages could be beneficial to increase more Li^+ storage sites to enlarge electrode-electrolyte contact area and relief volume structure change of the materials in the discharge and charge process of Li^+. However, the multi-shelled hollow SiO_2 with hierarchical pores have been rarely reported due to the multiformity and complexity of the multi-shelled hollow structure with hierarchical pores, and then it is a challenge to establish a preparation method with operability and controllability.

Herein, we first time synthesized the multi-shell hollow silica microspheres (MHSM) with hierarchically porous structure and controllable shell numbers (ranging from 1 to 3) through a simple sacrificial template method. As shown in Scheme 1, the carbonaceous microspheres (CMSs) are used as templates to absorb the precursor (sodium silicate). The shells numbers of SiO_2 microspheres with hierarchically pores can increase with the increasing amount of sodium silicate adsorbed into the templates during the calcination process. To reach multi-shell hollow and hierarchically porous structure, two points in the formation process are important and essential. One is that the appropriate concentration of absorbate is a key to control the shell numbers of the MHSM. The other is that SiO_3^{2-} anions absorbed into the CMSs could be acted as a "nano building-units" to form the hierarchically ordered SiO_2 nanoparticles resulting into the hierarchically porous nature. The hierarchically porous single-, double- and triple-shelled hollow microspheres are named as SHSM, DHSM and THSM, respectively. Functional investigation found that the THSM as the lithium ion battery anode possessed 750 mAh g^{-1} discharge capacity and non-obviously attenuate later at 100 mA g^{-1} current density after 500 cycles, which indicated that the cycling stability of SiO_2 materials as an anode material in the LIB can be improved. We believe multi-shell hollow silica microspheres with hierarchical pores may be advantageous in the practical application of high-performance lithium ion battery anode materials.

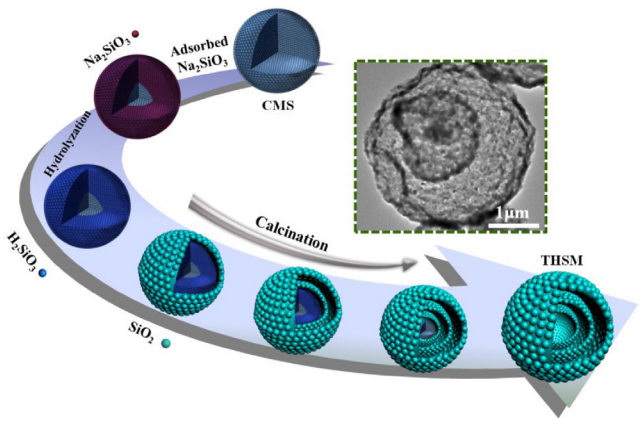

Scheme 1. The schematic of the formation mechanism for the multi-shell hollow silica spheres with hierarchically porous structure.

2. Experimental sections

2.1. Materials

All chemicals used in the study were of analytical grade and used without further purification. Sodium metasilicate nonahydrate ($Na_2SiO_3{\cdot}9H_2O$) was purchased from Shantou Xilong Chemical Co., Ltd. in China. Glucose anhydrous ($C_6H_{12}O_6$) was purchased from Deen Tianjin Chemical Reagent Co., Ltd. Absolute ethanol and ultrapure water were used for sample washing in the experiment.

2.2. Characterizations

The powder X-ray diffraction patterns of MHSM was characterized on a Bruker D8 & Advance X-ray powder diffractometer with graphite monochromatized CuKα (λ = 0.15406 nm). The FTIR spectrum was determined using a PerkinElmer Spectrum 400 Fourier transform infrared spectrometer in the wave number range of 4000–400 cm^{-1}. Field emission scanning electron microscopy (FESEM) analyses were performed using a SU8010 cold field emission scanning electron microscopy equipped with an Energy Dispersive Spectroscopy (EDS), which was used to observe the morphologies and elemental constitution of the products. The interior structure and particle size of samples was obtained by a JEM-2100 transmission electron microscope (TEM) equipped with a selected-area electron diffraction (SAED). HRTEM was used to analyze the size of particles and crystal of products. Samples of MSHM with hierarchically porous structure were prepared for a TEM by dripping 5 mL dilute alcohol solution onto the carbon-coated copper grids. N_2 absorption/desorption isotherms were generated at 77 K using a Micromeritics ASAP 2010 analyzer. The samples were firstly degassed at 300 °C for 6 h before analysis. The calculation of specific surface area made use of the Brunauer-Emmett-Teller (BET) model, and the pore size distribution was calculated from the adsorption branch of the isotherms by the Barret-Joyner-Halenda (BJH) model. The total pore volume was estimated from the amounts of N_2 adsorbed at a relative pressure (P/P_0) of 0.99.

2.3. Preparation of the MHSM with hierarchically porous structure

The synthesis process involves as follows: First, the templates CMSs were prepared using glucosum aqueous solution as reactants (3.6 g glucosum anhydricum dissolved with 30 mL high purity water) through hydrothermal reaction at the 180 °C for 12 h (Fig. S1). Then, newly prepared CMSs (20 mg) were dispersed in sodium silicate solution (50.0 mmoL L^{-1}), which was adjusted to faintly acid (pH = 5.00) with the hydrochlorate acid solution (1 mmoL L^{-1}). After ultrasonic dispersion for 15 min, the black suspension was aged for 8 h at 50 °C and then filtered, washed, and dried at 80 °C for 12 h. The resultant microspheres were heated to 450 °C for 3 h in air at the rate of 1 °C min^{-1}. Finally, the white powders were obtained. Based on the similar method, the SHSM and DHSM were synthesized when the concentration of precursor (sodium silicate) was respectively 12.5 mmoL L^{-1} and 25 mmoL L^{-1}.

2.4. Electrochemical measurement

The electrochemical measurement behavior of the as-prepared THSM with hierarchically porous structure was detected using the CR2032-type coin cell, assembled in an argon-filled glove box (CL800S). The working electrode is compounded by dissolving a

mixture, the active materials (THSM), conductive material, and binder (polyvinylidenefluoride) in a mass ratio of SiO_2/carbon/PVDF = 5:3:2, in the 1-Methyl-2-Pyrrolidone (NMP). The counter electrode of the LIB is lithium metal. A porous membrane (Celgard 2400) was used as the separator. The electrolyte of cells is fabricated by dissolving 1 M $LiPF_6$ in ethylene carbonate and diethyl carbonate (EC:DEC = 1:1, v:v). Galvanostatic charge-discharge and cycling performance measurements were performed on a LAND-CT2001A and cyclic voltammetry (CV) was performed on a CHI 660D. All electrochemical capacity values were calculated on the total electrode weight (carbon + SiO_2). The cycling capacity of the cells were examined in the voltage range between 0 V and 3 V at a current density of 100 mA g^{-1} and CV was performed using a scan rate of 0.01 mv s^{-1}. The loading mass and density of THSM on the electrodes (copper foil) were 3 mg and 1.95 mg/cm^3, respectively.

3. Results and discussion

3.1. Characterization of the MHSM with hierarchically porous structure

Fig. 1 shows the size and morphology of the SHSM, DHSM and THSM through the FESEM (field emission scanning electron microscopy), TEM (transmission electron microscope) and HRTEM (High-resolution TEM). The FESEM images show that the synthesized SiO_2 are the uniform and intact microspheres with the size about 3 μm in diameter (Fig. 1a, e and i). The corresponding magnified images of FESEM (Fig. 1b, f and j) and TEM (Fig. 1c, g and k) analysis can clearly illustrate the single-, double- and triple-shelled structure of the hollow SiO_2 microspheres obtained, respectively. From the TEM images, it can be observed that the obvious contrast between the dark edge and pale center also indicates their hollow nature. Furthermore, we can find that the multi-shells of the SiO_2 microspheres consist of the SiO_2 nanoparticles, resulting into the porous structure of the shells. The regions of light contrast between individual SiO_2 nanoparticles further indicate the presence of mesopores within the shells (Fig. 1d, h and l). The porous structure of the shells can provide a three dimensional network for the hollow SiO_2 microspheres. Moreover, the fuzzy diffraction rings in the SEAD patterns indicate the amorphous form of the samples (the inset of Fig. 1d, h, l). However, the multi-shell hollow and hierarchical porous structure can't obtain with both higher (100 mmoL L^{-1}) or lower concentration (7 mmoL L^{-1}) of Na_2SiO_3 loaded into CMSs (Fig. S2). From the results, we could achieve hierarchically porous hollow SiO_2 spheres with different interior structures though controlling the concentration of the precursors loaded into the templates. Thermogravimetric Analysis (TGA) further analysis the content of SiO_2 in SHSM, DHSM and THSM, respectively. From Fig. S3, we can observe the appearance of plateau before 550 °C. The result illustrated the CMSs were completely removed before 550 °C. Otherwise, the result could also indicate that the shell number of sample increased from 1 to 3 with the increase of the precursors' concentration.

The composition of MHSM with hierarchically porous structure is confirmed by EDS, XRD and FTIR, respectively (Fig. 2). The EDS element mapping micrographs of Si and O illustrate that the element Si and O uniformly distribute in the surface of THSM (Fig. 2b, c, d and e), as do the element mappings of SHSM and DHSM (Fig. S4). XRD pattern of the materials shows a weak peak at about 23°, confirming the presence of pure amorphous silica (Fig. 2f). In the FTIR spectra (Fig. 2g), the bands at 1075 cm^{-1} and

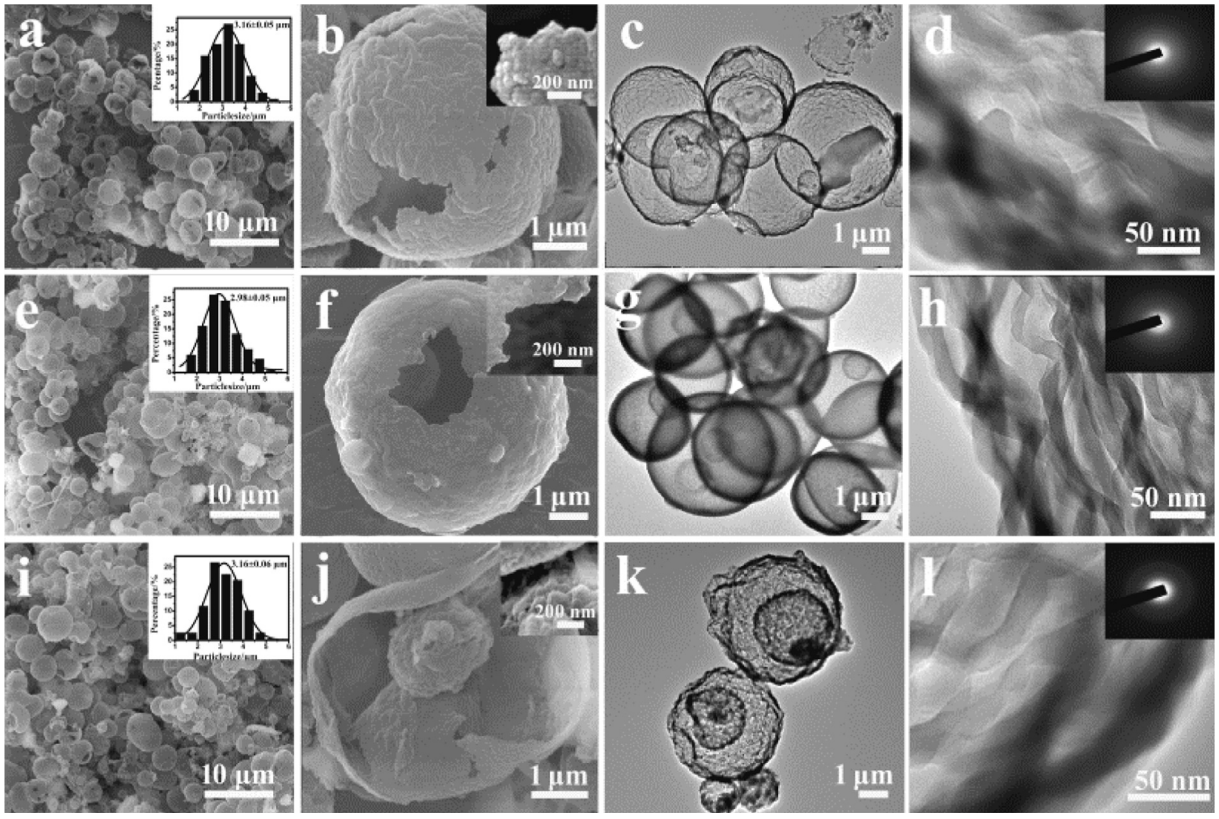

Fig. 1. The morphology of MHSM with hierarchically porous structure. FESEM (a, e, i), the image magnification of FESEM (b, f, j), TEM (c, g, k) and the HRTEM (d, h, l) of the single-, double-, triple-shell hollow silica microspheres with hierarchically porous structure, respectively. The inset in FESEM corresponding with the particle size distribution and the detail enlarged drawing, in the HRTEM meeting with the SAED of samples.

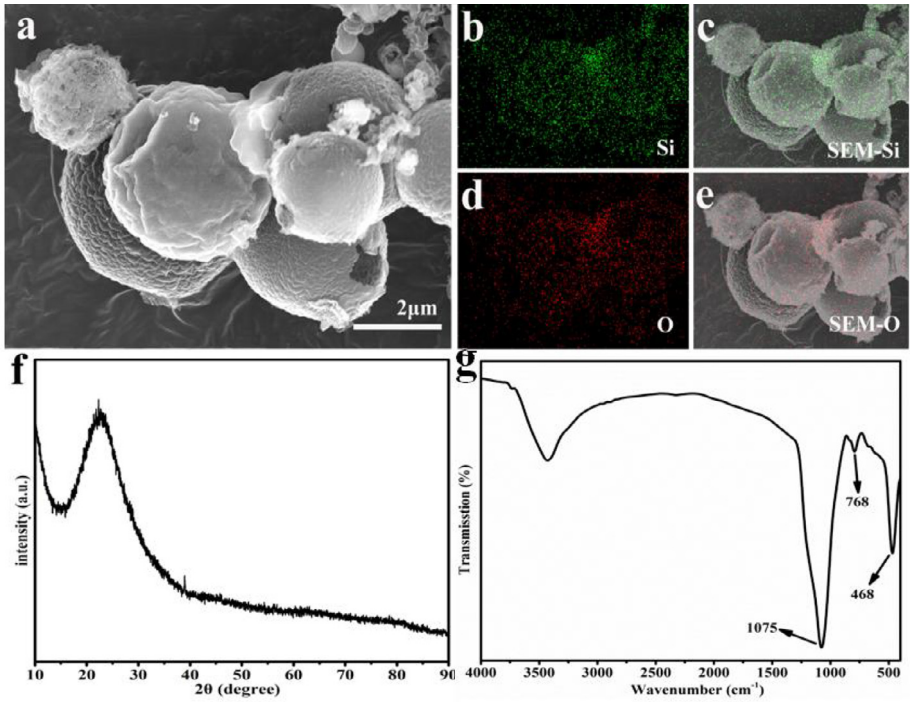

Fig. 2. FESEM of the THSM with hierarchically porous structure (a) and the EDS element mapping micrographs of Si (b), Si-SEM (c), O (d) and O-SEM (e), XRD (f) and FTIR (g) of the THSM with hierarchically porous structure.

788 cm^{-1} illustrate the Si-O-Si asymmetric stretching vibrations and the Si-O-Si symmetric stretching vibrations, respectively. The banding vibration of SiO_4 at 468 cm^{-1} is the third characteristic peak of the amorphous silica [24].

The hierarchically porous structure of the multi-shell hollow SiO_2 microspheres is further confirmed by the nitrogen adsorption measurements. From the nitrogen adsorption isotherms of the SHSM, DHSM and THSM (Fig. 3a), we can distinctly recognize the existence of typical type IV isotherm and type III hysteresis loop at the relatively high pressure (P/P_0) about 0.9, indicating the characteristic of complex porous structure [25]. The pore size distribution curve (BJH model) of the MHSM shows three peaks centered at about 2, 10 nm and 88 nm for each sample, representing the existence of micropores, mesopores and macropores respectively (Fig. 3b). The results indicate the presence of the hierarchically porous structure of the multi-shell SiO_2, which contains three kinds of pores in the materials. The Brunauer-Emmett-Teller (BET) model was applied to calculate the specific surface area of the SHSM, DHSM and THSM, and the detailed results are listed in the Table 1. It can be clearly seen that the specific surface area and pore volume of the samples increase with the increasing of the shell numbers, indicating a relatively large surface-to-volume ratio of the samples, which could not only supply more adsorption active sites but also reduce the transport lengths between mass and charge transport.

Table 1
Specific surface area, pore volume and average pores size of the MHSM with hierarchically porous structure.

Samples	BET surface area ($m^2 \cdot g^{-1}$)	Pore volume ($cm^3 \cdot g^{-1}$)	Pore size (nm)
SHSM	3.22	0.03	2.32, 10.19 and 86.82
DHSM	14.80	0.06	2.17, 11.72 and 88.16
THSM	34.66	0.14	2.07, 10.09 and 87.35

To discuss the evolution processes of the multi-shell hollow structure, the temperature-dependent experiments were carried out (Fig. 4). From the TEM images, it can be find that the shell numbers of hollow SiO_2 are controlled by altering the loading amount of Na_2SiO_3 into the templates, which could be achieved by adjust-

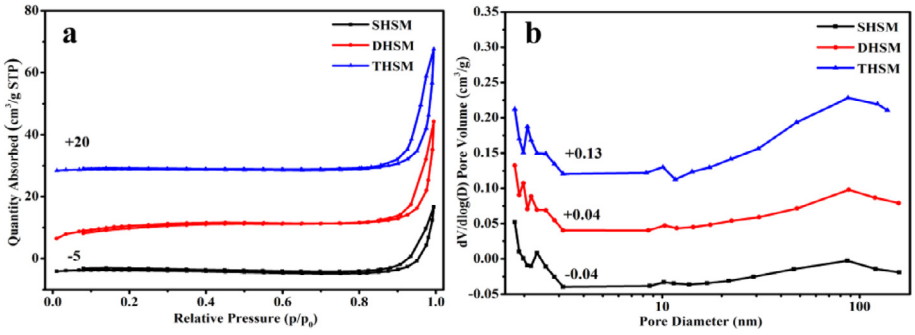

Fig. 3. N_2 adsorption-desorption isotherms (a) and relating with pore-size distribution curves (b) of the THSM with hierarchically porous structure.

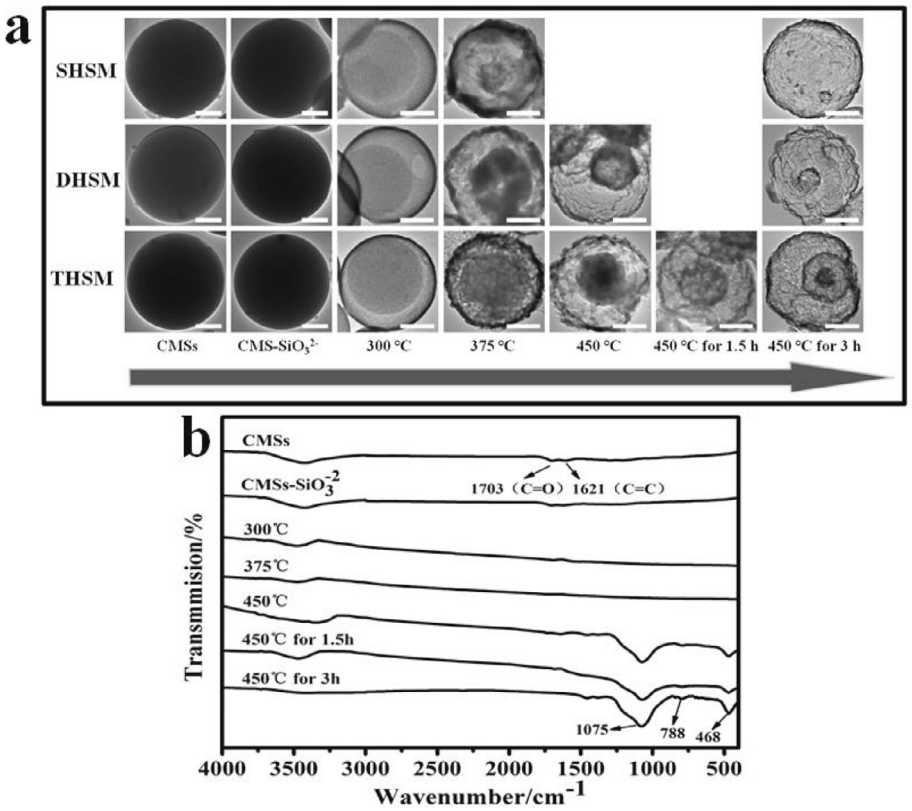

Fig. 4. (a) Evolution processes of the MHSM with hierarchically porous structure. TEM images of the CMSs, the CMSs-SiO_3^{2-} (the CMS adsorbed with sodium silicate) and the CMSs-SiO_3^{2-} after calcined to 300 °C, 375 °C, 450 °C, 450 °C for 1.5 h and 450 °C for 3 h at a heating rate of 1 °C/min. The scale bars are 1 μm. (b) The FTIR spectra at different calcination stages of products obtained during the preparation process of MHSM with hierarchical pores.

ing the adsorption concentration of Na_2SiO_3 into the CMSs under same adsorption conditions. The less amount and infiltration depth of Na_2SiO_3 incorporated into the CMSs could result in less amount of H_2SiO_3 came from the hydrolysis of Na_2SiO_3. During the calcination process, the outer layer of the CMSs combusted, and at the same time, the H_2SiO_3 loaded into the outer layer of the CMSs gradually decomposed into SiO_2 nanoparticles which were regarded as nano-building units. The SiO_2 nanoparticles in the outer of the outmost silica shell are easier to grow up than the SiO_2 nanoparticles in the inner region of the outmost silica shell because that the SiO_2 nanoparticles could be facilitated by the higher temperature around the outmost silica shell. According to the inside-out Ostwald Ripening, the less-crystalline of silica nanoparticles in the inner region of the outmost silica shell gradually dissolved to improve the growth of big nanoparticles in the outer of the outmost silica shell. Otherwise, due to the different contraction rates of the different materials, the outer silica shell and the inner CMSs core are gradually separated along with continuous conduction of heat from outer surface to inner surface of CMSs. Consequently, the first shell can be obtained (the samples obtained at 300 °C and 375 °C during the formation process of SHSM in Fig. 4a), and then SHSM could be obtained by further heating which could result in the complete combustion of CMSs core (the sample calcined at 450 °C for 3 h during the SHSM formation process in Fig. 4a).

With the increase of the adsorption concentration of Na_2SiO_3 into the CMSs, the H_2SiO_3 could diffuse and infiltrate into the deep layer of the CMSs at the same above adsorption condition. Due to a temperature lag resulting from the slow heating up procedure, H_2SiO_3 in the interior do not involve in the outer shell of SiO_2 and they are still immersed into the interior of the templates (the sample DHSM heated from 300 °C to 450 °C in Fig. 4a). Based on aforesaid situation of the SHSM, the inside-out Ostwald ripening process and the different shrinking rate of both materials promoted the formation of the first shell silica. When heat further passed into the deeper inner of CMSs, the core-shell separation process during the silica shell and CMSs core recurred and further formed the second shell silica.

Further increasing the adsorption concentration of Na_2SiO_3 into the CMSs, the H_2SiO_3 could diffuse and infiltrate into the deeper layer of the CMSs. Based on the formation process of SHSM and DHSM, the triple-shell hollow silica microspheres with hierarchical pores can been obtained (the samples obtained during the formation process of THSM in Fig. 4a). The corresponding FTIR spectrum at different calcination stages of products indicate that the formation of SiO_2 nanoparticles is accompanied with the combustion of the CMSs during the heating process (Fig. 4b). In summary, the inside-out Ostwald Ripening process could result in the formation of the nanoparticles and shells of SiO_2. Otherwise, the different contraction rates between CMSs and SiO_2 could keep the outer SiO_2 shell and the inner CMSs core apart along with the increase of temperature and the heating time (Scheme 1).

3.2. Electrochemical properties of THSM with hierarchically porous structure

Due to the multi-shelled hierarchically porous structure and large specific surface area of THSM, the electrochemical properties are further evaluated by Coin-type half cells (2032-type). The representative cyclic voltammograms (CV) curves of the THSM are shown in Fig. 5a. There is a weak reduction peak at around 0.75 V in the first cycle. The formation of the peak may be caused by the decomposition of electrolyte and the formation of the solid

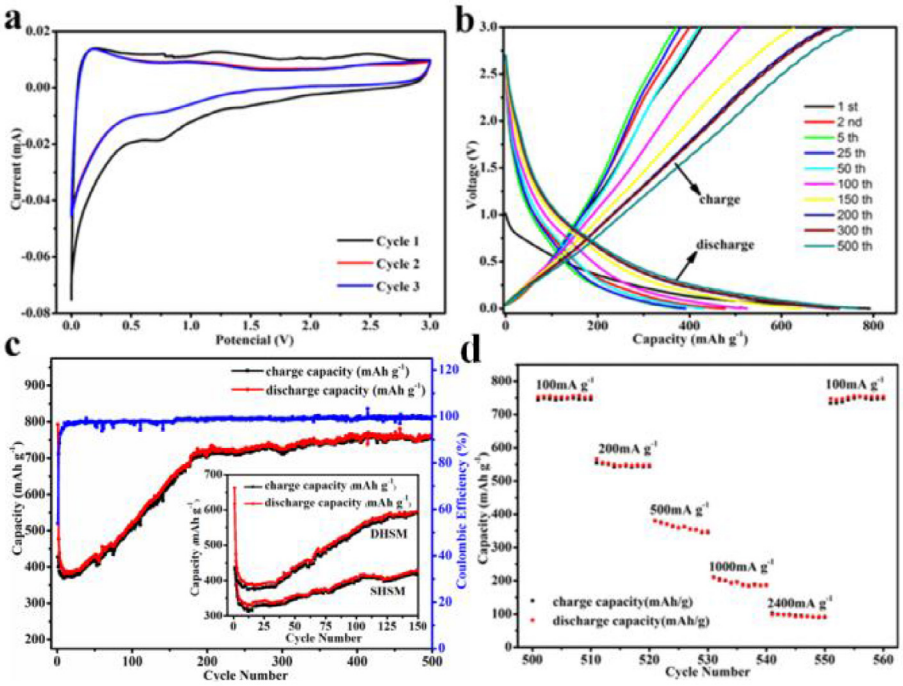

Fig. 5. (a) Cyclic voltammetry of the THSM at a scan rate of 0.1 mV s^{-1}. (b) the charge-discharge curves of THSM at 100 mA g^{-1} under different cycles. (c) the cycle profile of THSM as LIB anodes at current density of 100 mA g^{-1} (the inset corresponding with the cycle profile of SHSM and DHSM as LIB anodes at current density of 100 mA g^{-1}). (d) rate data of THSM under different current density over 500 cycles. All of the measurements were conducted using a voltage window of 0–3.0 V.

electrolyte interface (SEI) layer [10,11]. Fig. 5b reveals that the charge-discharge profiles of THSM for different cycles at constant current density of 100 mA g^{-1}. There is a voltage plateaus appearing at 0.75 during the discharge processes, which is in accordance with the CV (Fig. 5a). From Fig. 5c, we can see that the capacity changing curve has three stages. Stage (I): from first cycle to 9th cycles, an obvious rapidly drop in the specific capacity was recorded. The discharge capacity at the first cycle was 792.5 mAh g^{-1}, while the first charge delivered a capacity of 427.2 mAh g^{-1} (Fig. 5c). The 46.09% initial capacity loss (or the coulombic efficiency (CE) around 53.91%) is induced by the inevitable formation of solid electrolyte interface (SEI) and by the irreversible electrochemical reaction between Li and THSM. Stage (II), in the range of 11–30 cycles, the specific capacity of the amorphous THSM anode stabilized, and the voltage profiles overlap approximately in the whole voltage range (Fig. 5c) exhibiting coulombic efficiencies approaching 99%. The result clearly indicated that the electrochemical reaction became reversible, which resulted from that the THSM would be reduced to Si. Stage (III): beyond 30th cycles, the THSM anodes exhibited a gradual enhancement of lithium storage capacity.

The anomalous increase in the charge-discharge curve can be observed from 380 mAh g^{-1} (50th), 490 mAh g^{-1} (100th), 600 mAh g^{-1} (150th) to 700 mAh g^{-1} (200th) and followed by a nearly constant capacity at 750 mAh g^{-1} till the 500th cycles. The following reasons provided an conjecture of the unusual capacity rise with THSM anodes. First, the increase of electrical conductivity of THSM anodes contributed to the capacity rise with THSM anodes, which resulted from the gradual reduction of SiO_2 (poor electrical conductivity) to Si (good electrical conductivity) in the electrochemical reaction between Li and SiO_2. Second, the improvement of the Li^+ diffusion kinetics could also contribute to the capacity rise with THSM anodes because the Li^+ diffusion path could be shorten by the special multi-shell hollow and hierarchically porous structure. In addition, the phenomenon of the unusual capacity rise could result from the interfacial Li storage and the THSM with the disordered or amorphous structure. [26–31] Third, the insertion of Li formed Li_4SiO_4-like defects that were irreversible at Si/SiO_2 interfaces. However, these structures increase the volume fractions of Si and Li_4SiO_4, and increase the lithium storage capacity when formed at Si/SiO_2 interface [27]. Meantime, we find the capacity of THSM (750 mAh g^{-1}) was higher than the capacity of SHSM (600 mAh g^{-1}) and DHSM (410 mAh g^{-1}) which were shown in the inset of Fig. 5C. The results indicate the special capacity of sample increased gradually with the increasing shell of amorphous silica. The advantage of capacity for the MHSM is attributed mainly to the special multi-shell hollow structure with hierarchical pore which can caused the shorter diffusion path of Li^+. In other word, the special multi-shell hollow structure with hierarchical pore could enhance the reactivity in Li^+ diffusion kinetics. After 500 cycles, the current densities increased to 200, 500, 1000 and 2400 mA g^{-1} (Fig. 5d), the discharge capacities of THSM were 550, 350, 200 and 100 mAh g^{-1}, respectively. The special capacity of the THSM can go back and still retained in the rate capacity of 750 mAh g^{-1} after 550 cycles at 100 mA g^{-1}. The results indicate that the THSM has outstanding cycling stability after undergoing different current densities.

To explore the Li^+ storage property and the stability of this structure, the evolution of morphology and structure of THSM during the charge-discharge processes are further investigated. The FESEM and TEM images of THSM electrodes after 500 cycles were shown in Fig. S5. The FESEM image shows a large number of intact multi-shell silica microspheres with the size around 3 μm in diameter (Fig. S5a). The TEM image further shows the multi-shell hollow structure of samples can be maintained after 500 cycles (Fig. S5b). And the THSM can be observed by the detail enlarged drawing in the right inset of TEM, Furthermore, the THSM display the typical SAED patterns of polycrystalline nanostructure, in which multiple concentric cycles can be shown (the left inset of

Table 2
Comparison of the lithium-storage performance between the THSM and reported SiO_2-based anode materials previously.

SiO_2-baced anodes	Capacity (mAh g^{-1})	Cycles	Current density (mA g^{-1})	Potential range (V)	Reference
THSM with hierarchical pores	750	>500	100	0–3	This work
SiO_2/Cu/polyacrylonitrile-C composite	537	≈180	110	0–3	[33]
Carbon-coated SiO_2 nanoparticles	>500	50	50	0–3	[34]
Dual-porosity SiO_2/C Nanocomposite	635.7	200	100	0.01–2.5	[26]
SiOx@C composite nanorods	≈720	350	100	0–3	[35]
Hollow porous SiO_2 nanocubes	919	30	100	0–3	[13]
SiO_2-NT/G network	1145.3	100	100	0.01–3	[16]

Fig. S5b). The phenomenon results from the change of crystallinity of silica during charge-discharge cycle processes.

Based on the work done of others [13,14,26], we calculated the reaction between Li^+ and SiO_2 described as follow:

$$2SiO_2 + 4Li^+ + 4e^+ \rightarrow Li_4SiO_4 + Si; \quad (1)$$

$$SiO_2 + 4Li^+ + 4e^+ \rightarrow 2Li_2O + Si; \quad (2)$$

$$Si + xLi^+xe^+ \rightarrow Li_xSi; \quad (3)$$

$$Li_xSi \rightarrow Si + xLi^+ + xe^+; \quad (4)$$

The Eqs. (1) and (2) expound the conversion of SiO_2 and Si among the Li^+ insertion/desertion between Li^+ and THSM. The Eqs. (3) and (4) indicate the alloy mechanism of Si and Li^+. Additionally, on the base of the reaction (1), (3) and (4) or the reaction of (2), (3) and (4), the theoretical special capacity of SiO_2 was 980 mAh g^{-1} and 1960 mAh g^{-1}, respectively [10,13]. And so, we applied X-ray photoelectron spectroscopy (XPS) to speculate that the reaction process between Li^+ and THSM before and after discharged to 0 V (Fig. 6). Fig. 6a shows the spectra of Si 2p for the THSM before and after discharged to 0 V. The peak located in the 103.69 eV, assigned to amorphous silica, is shifted to 102.88 eV and broadened after discharged to 0 V. XPS analysis shows that the Si 2p peak is two chemical state of Si. One is the peak at 103.3 eV corresponding with the formation of Li_4SiO_4 (the blue peak at Fig. 6a), and the other is similar to the Li-Si alloy at 101 eV (the pink peak at Fig. 6a), which could indicate the appearance of reversible reaction between Li^+ and Si. Additionally, the O 1s (Fig. 6b) spectra reveals the red-shifts phenomenon of sample after discharged to 0 V, attributing to the weaken situation of the bonding between Si and O. The peak of as-prepared silica sample at 532.69 eV shifts towards the peak at 531.8 eV after discharged to 0 V, which is matching with the variation of the spectra of Si 2p. However, when the compounds are recharged to 3 V, the peak at 531.77 eV is not distinctly shifted but fitted in with the discharged peak, which is suggesting to be the irreversible change duo to the formation of Li_4SiO_4 [10,13,26,32].

Finally, comparing with the lithium-storage performance of previously reported SiO_2-based anode materials, the THSM with hierarchically porous structure show high charge-discharge cycle reversible capacity and remarkable cycle stable performance, which is held in 750 mAh g^{-1} (specific capacity) over 500 cycles (from Table 2). Such the good performance of the THSM with hierarchically porous structure might be attributed to the hollow multi-shell structure and hierarchically porous structure. The unique structure can not only provide the more extraction and insertion sites of Li^+ but also enhance the stability of SiO_2 in the charge-discharge process of lithium ion. In addition, the structure can also produce more extra spaces and storage sites in the internal cavity of silica microspheres to accommodate the volume expansion and mechanical tension change in the rapid diffusion process between Li^+ and silica microspheres. Despite all this, the multi-shell hollow structure with hierarchical pores could further been optimized to improve cyclic stability and lithium-storage capacity of THSM.

4. Conclusion

In summary, the multi-shell hollow silica microspheres with hierarchically porous structure were for the first time obtained by a simple sacrificial template method. The MHSM as anodes materials for lithium ion battery showed the prominent cycle stability, which was distinguished by a retaining situation of cycle performance examination under different current density, and high reversible capacity. The performances resulted from the unique hollow multi-shell with hierarchically porous structure, which guaranteed the easy reaction between lithium ion and silica on the shell surface of MHSM with hierarchically porous structure through reducing their reaction path and created a "buffer" for the silica volume expansion during cycling.

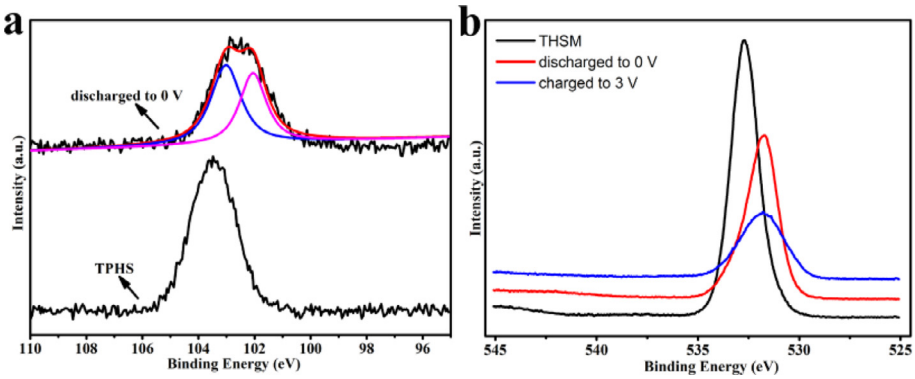

Fig. 6. The Si 2p (a) and O 1s (b) XPS spectra of THSM with hierarchically porous structure before and after discharged to 0 V, respectively.

Acknowledgements

This work was financially supported by the National Science Foundation of China (Grant no. 21271065); NFSC-Henan Talent Training United Fund (Grant no. U1204519); Science and Technology Innovation Support Plan of the University of Henan province (Grant no. 14HASTIT010) and Postdoctoral Science Foundation of China (Project No. 2016M592294).

Appendix A. Supplementary data

Supplementary data associated with this article can be found, in the online version, at http://dx.doi.org/10.1016/j.cej.2017.04.108.

References

[1] M. Armand, J.M. Tarascon, Building better batteries, Nature 451 (2008) 652–657.
[2] P.G. Bruce, B. Scrosati, J.M. Tarascon, Nanomaterials for rechargeable lithium batteries, Angew. Chem. Int. Ed. 47 (2008) 2930–2946.
[3] J.W. Choi, D. Aurbach, Promise and reality of post-lithium-ion batteries with high energy densities, Nat. Rev. Mater. 1 (2016) 16013–16028.
[4] Q.F. Xiao, M. Gu, H. Yang, B. Li, C.M. Zhang, Y. Liu, F. Liu, F. Dai, L. Yang, Z.Y. Liu, X.C. Xiao, G. Liu, P. Zhao, S.L. Zhang, C.M. Wang, Y.F. Lu, M. Cai, Inward lithium-ion breathing of hierarchically porous silicon anodes, Nat. Commun. 6 (2015) 8844–8851.
[5] C.K. Chan, H.L. Peng, G. Liu, K. Mcllwrath, X.F. Zhang, R.A. Huggins, Y. Cui, High-performance lithium battery anodes using silicon nanowires, Nat. Nanotechnol. 3 (2008) 31–35.
[6] Z.D. Lu, N. Liu, H.W. Lee, J. Zhao, W.Y. Li, Y.Z. Li, Y. Cui, Nonfilling carbon coating of porous silicon micrometer-sized particles for high-performance lithium battery anodes, ACS Nano 9 (2015) 2540–2547.
[7] H. Wu, G. Chan, J.W. Chol, L. Ryu, Y. Yao, M.T. McDowell, S.W. Lee, A. Jackson, Y. Yan, L.B. Hu, Stable cycling of double-walled silicon nanotube battery anodes through solid–electrolyte interphase control, Nat. Nanotechnol. 7 (2012) 309–314.
[8] H. Wu, Y. Cui, Designing nanostructured Si anodes for high energy lithium ion batteries, Nanotoday 7 (2012) 414–429.
[9] M. Miyachi, Y. Hironori, K. Hidemasa, O. Tomoyuki, S. Masato, Analysis of SiO_2 anodes for lithium-ion batteries, J. Electrochem. Soc. 152 (2005) A2089–A2091.
[10] B.K. Guo, J. Shu, Z.X. Wang, H. Yang, L.H. Shi, Y.N. Liu, L.Q. Chen, Electrochemical reduction of nano-SiO_2 in hard carbon as anode material for lithium ion batteries, Electrochem. Commun. 10 (2008) 1876–1878.
[11] B. Gao, S. Sinha, L. Fleming, O. Zhou, Alloy formation in nanostructured silicon, Adv. Mater. 13 (2001) 816–819.
[12] Q. Sun, B. Zhang, Z.W. Fu, Lithium electrochemistry of SiO_2 thin film electrode for lithium-ion batteries, Appl. Surf. Sci. 254 (2008) 3774–3779.
[13] N. Yan, F. Wang, H. Zhong, Y. Li, Y. Wang, L. Hu, Q.W. Chen, Hollow porous SiO_2 nanocubes towards high-performance anodes for lithium-ion batteries, Sci. Rep. 3 (2013) 1568–1573.
[14] W.-S. Chang, C.-M. Park, J.-H. Kim, Y.-U. Kim, G. Jeong, H.-J. Sohn, Quartz (SiO2): a new energy storage anode material for Li-ion batteries, Energy Environ. Sci. 5 (2012) 6895–6899.
[15] H. Wang, P. Wu, H.M. Shi, W.Z. Tang, Y.W. Tang, Y.M. Zhou, P.L. She, T.H. Lu, Hollow porous silicon oxide nanobelts for high-performance lithium storage, J. Power Sources 274 (2015) 951–956.
[16] H. Wang, P. Wu, M.T. Qu, L. Si, Y.W. Tang, Y.M. Zhou, T.H. Lu, Highly reversible and fast lithium storage in graphene-wrapped SiO_2 nanotube network, ChemElectroChem 2 (2015) 508–511.
[17] X.M. Ma, X.T. Zhang, L. Yang, K. Wang, K. Jiang, Z.P. Wei, Y.M. Guo, An unusual temperature gradient crystallization process: facile synthesis of hierarchical ZnO porous hollow spheres with controllable shell numbers, CrystEngComm 14 (2014) 7933–7941.
[18] X.M. Ma, X.T. Zhang, L. Yang, G. Wang, K. Jiang, G. Wu, W.G. Cui, Z.P. Wei, Tunable construction of multishelled hollow carbonate nanospheres and its potential applications, Nanoscale 8 (2008) 8687–8695.
[19] B. Fang, J.H. Kim, M.S. Kim, J.S. Yu, Hierarchical nanostructured carbons with meso-macroporosity: design, characterization, and applications, Acc. Chem. Res. 46 (2012) 1397–1406.
[20] H. Ren, R.B. Yu, J.Y. Wang, Q. Jin, M. Yang, D. Mao, D. Kisailus, H.J. Zhao, D. Wang, Multishelled TiO_2 hollow microspheres as anodes with superior reversible capacity for lithium ion batteries, Nano Lett. 14 (2014) 6679–6684.
[21] L. Zhang, H.B. Wu, Y. Yan, X. Wang, X.W. Lou, Hierarchical MoS_2 microboxes constructed by nanosheets with enhanced electrochemical properties for lithium storage and water splitting, Energy Environ. Sci. 7 (2014) 3302–3306.
[22] J.Y. Wang, N.L. Yang, H.J. Tang, Z.H. Dong, Q. Jin, M. Yang, D. Kisailus, H.J. Zhao, Z.Y. Tang, D. Wang, Accurate control of multishelled Co_3O_4 hollow microspheres as high-performance anode materials in lithium-ion batteries, Angew. Chem. Int. Ed. 52 (2013) 6417–6420.
[23] X. Wang, X.L. Wu, Y.G. Guo, Y.T. Zhong, X.Q. Cao, Y. Ma, J.N. Yao, Synthesis and lithium storage properties of Co_3O_4 nanosheet-assembled multishelled hollow spheres, Adv. Funct. Mater. 20 (2010) 1680–1686.
[24] M. Sasidharan, D. Liu, H. Gunawardhana, M. Yoshio, K. Nakashima, Synthesis, characterization and application for lithium-ion rechargeable batteries of hollow silica nanospheres, J. Mater. Chem. 21 (2011) 13881–13888.
[25] K.S.W. Sing, Reporting physisorption data for gas/solid systems with special reference to the determination of surface area and porosity, Pure Appl. Chem. 54 (1982) 01–2218.
[26] H.H. Li, X.L. Wu, H.Z. Sun, K. Wang, C.Y. Fan, L.L. Zhang, F.M. Yang, J.P. Zhang, Dual-porosity SiO_2/C nanocomposite with enhanced lithium storage performance, J. Phys. Chem. C 119 (2015) 3495–3501.
[27] C. Ban, B.B. Kappes, Q. Xu, C. Engtrakul, C.V. Ciobanu, A.C. Dillon, Y.F. Zhao, Lithiation of silica through partial reduction, Appl. Phys. Lett. 100 (2012) 243905.
[28] Y.Z. Jiang, D. Zhang, Y. Li, T.Z. Yuan, N. Bahlawane, C. Liang, W.P. Sun, Y.H. Lu, M. Yan, Amorphous Fe_2O_3 as a high-capacity, high-rate and long-life anode material for lithium ion batteries, Nano Energy 4 (2014) 23–30.
[29] C. Masarapu, V. Subramanian, H.W. Zhu, B.Q. Wei, Long-Cycle electrochemical behavior of multiwall carbon nanotubes synthesized on stainless steel in Li Ion batteries, Adv. Funct. Mater. 19 (2009) 1008–1014.
[30] D.H. Liu, H.Y. Lü, X.L. Wu, B.H. Hou, F. Wan, S.D. Bao, Q.Y. Yan, H.M. Xie, R.S. Wang, Constructing the optimal conductive network in MnO-based nanohybrids as high-rate and long-life anode materials for lithium-ion batteries, J. Mater. Chem. A 3 (2015) 19738–19746.
[31] Y.M. Sun, X.L. Hu, W. Luo, F.F. Xia, Y.H. Huang, Reconstruction of conformal nanoscale MNO on graphene as a high-capacity and long-life anode material for lithium ion batteries, Adv. Funct. Mater. 23 (2013) 2436–2444.
[32] B. Philippe, R. Dedryvère, J. Allouche, F. Lindgren, M. Gorgoi, H. Rensmo, D. Gonbeau, K. Edström, Nanosilicon electrodes for lithium-ion batteries: interfacial mechanisms studied by hard and soft X-ray photoelectron spectroscopy, Chem. Mater. 24 (2012) 1107–1115.
[33] M.Q. Li, J. Li, K. Li, Y. Zhao, Y.G. Zhang, D. Gosselink, P. Chen, SiO_2/Cu/polyacrylonitrile-C composite as anode material in lithium ion batteries, J. Power Sources 240 (2013) 659–666.
[34] Y. Yao, J.J. Zhang, L.G. Xue, T. Huang, A.S. Yu, Carbon-coated SiO_2 nanoparticles as anode material for lithium ion batteries, J. Power Sources 196 (2011) 10240–10243.
[35] Y.R. Ren, M.Q. Li, Facile synthesis of SiOx@C composite nanorods as anodes for lithium ion batteries with excellent electrochemical performance, J. Power Sources 306 (2016) 459–466.